Determination of critical layer thickness and strain tensor in $In_xGa_{1-x}As/GaAs$ quantum-well structures by x-ray diffraction

Y. C. Chen and P. K. Bhattacharya
Solid State Electronics Laboratory, Department of Electrical Engineering and Computer Science, The University of Michigan, Ann Arbor, Michigan 48109-2122

(Received 22 October 1992; accepted for publication 27 February 1993)

We have used the double-crystal x-ray rocking curve technique to determine lattice constant, strain relaxation, thickness, and critical thickness of a thin $In_xGa_{1-x}As$ layer embedded in GaAs. In this work we have measured and analyzed x-ray data over a wide scan angle ($\sim$2.0°). This allows the simultaneous determination of buried layer thickness and strain. The measurement results were analyzed by the dynamical diffraction theory. The critical thickness for an InGaAs layer embedded in GaAs obtained from x-ray data is shown to be larger than that predicted by the force balance model. The strain tensors as a function of layer thickness are also analyzed for the buried $In_xGa_{1-x}As$ of different x values.

I. INTRODUCTION

There are a number of semiconductor devices whose active regions consist of strained layers buried under one or more layers of different composition and thickness. In these devices it is crucial to determine the structural parameters such as layer thickness, lattice strain, strain relaxation, and critical thickness which ultimately determine dislocation density, band structure and band gap, transport and optical properties, and device performance.

Double-crystal x-ray diffraction technique has been widely used to characterize the structural properties of semiconductors. Recent advances in epitaxial techniques such as molecular beam epitaxy (MBE) have allowed the synthesis of near perfect semiconductor heterostructures, both strained and lattice matched. The x-ray wave fields in these structures are usually coherently related and the resultant Pendellösung fringes can be easily observed. These fringes and the Bragg peaks contain information on the structural parameters. However, when multiple layers are put together, the Pendellösung fringes from each individual layer are modulated by others, resulting in rather complicated rocking curves.[1–3] The rocking curve becomes even more complex when a structure involves layers of graded strain. In these cases, the structural parameters must be determined by fitting the simulated and measured rocking curves.

For studying strain and strain relaxation of a buried layer, one can use the *ABA* structure in which a thin layer of composition B is sandwiched between thicker layers of composition A. This structure is very useful for understanding the origin of the Pendellösung interference phenomena and many authors[2,4,5] have suggested that the structural parameters of an *ABA* structure can be determined from the interference profile in the vicinity of the Bragg peak of A. It has been pointed out that[5] (1) if we know precisely the lattice spacing of A and B then the thickness of B can be determined with a precision of $\pm\Delta t/4$ but with an uncertainty of some multiple of Δt ($\Delta t = d^2/\delta d$, where d is the lattice spacing and δd is the difference between the lattice spacings of layers A and B); (2) if we know precisely the number of lattice planes of B, then the lattice spacing can be estimated to an accuracy of $d/4$ with an uncertainty of some multiple of d. However, when we lack precise knowledge of both the plane spacings and the layer thickness, examining only the angular region of the Bragg peak of A fails to provide any useful information. This deficiency can be remedied by using a large scan angle to cover the Bragg peaks of both layers A and B and the associated fringes. The lattice parameters and layer thicknesses can then be obtained without too much uncertainty.

In the present study the double-crystal x-ray rocking curve technique has been used to characterize a series of MBE-grown strained $In_xGa_{1-x}As/GaAs$ heterostructures in which an $In_xGa_{1-x}As$ layer is sandwiched between a GaAs cap ($\sim$2000 Å) and a thick GaAs substrate. The results have been analyzed by the dynamical diffraction theory. We have measured and analyzed x-ray data over a wide scan angle ($\sim$2.0°). This allows the simultaneous and accurate determination of buried layer thickness and strain tensor. In addition, we can also determine the critical layer thickness and strain relaxation of buried layers.

II. EXPERIMENT

A computer-controlled high-resolution double-crystal x-ray diffractometer was used to obtain the rocking curves. The x-ray source is generated from a conventional copper target. A $\sim$0.2 mm$\times$1 mm slit 15 cm away from the silicon first crystal was used to improve the collimation and monochromatic property of the x-ray beam. The slit is narrowed down from both sides such that the tails of the intensity profile of the x-ray source are blocked and the intensity is about one third of that without the slit. This arrangement reduces the angular divergence of the x-ray beam incident on the sample crystal and allows the revelation of very fine features in the rocking curves. Slow scan also helps to improve the signal to noise ratio. For example, in the constant scan-speed mode, the standard deviation of the measured intensity is proportional to the square root of scan speed.

 0021-8979/93/117389-06$06.00 © 1993 American Institute of Physics

The experimental samples consist of a series of strained $In_xGa_{1-x}As/GaAs$ heterostructures in which an $In_xGa_{1-x}As$ layer is sandwiched between GaAs layers. The samples were grown on (100) GaAs by MBE. After oxide desorption a 2000 Å GaAs layer was first deposited at 600 °C. The growth was then interrupted for 90 s to allow the substrate temperature to ramp down to 520 °C. The InGaAs buried layer and a 2000 Å GaAs cap were then grown in sequence. The substrate temperature was set to 600 °C right after the growth of InGaAs without interruption. Pregrowth calibration of growth rates and compositions agreed with post-growth double-crystal x-ray data to an accuracy of 95%. For $In_xGa_{1-x}As$ with $x=0.2$, the Bragg peak of the buried InGaAs layer can be seen in logarithmic scale even when the layer is as thin as 150 Å. For smaller x, the minimum InGaAs thickness for observing its Bragg peak is larger.

III. X-RAY DIFFRACTION FROM MULTILAYERED HETEROSTRUCTURES

Because of the complex nature of the measured x-ray rocking curves, numerical simulations are usually required to extract the structural parameters. Kinematic,[6] semikinematic,[7] and dynamical[8–10] diffraction theories have been used for the analysis. Before going into the numerical simulations, it is helpful to examine some analytical approximations in order to gain physical insight into the interference patterns. In the literature, both the Darwin–Prins[11] and the Taupin–Takagi[12,13] equations have been applied to analyze x-ray rocking curves. In fact, as shown in the Appendix, the two formulations are equivalent under the assumption that the crystal is a continuous medium. The Taupin–Takagi equations can be combined into a single differential equation of X (the normalized amplitude ratio of the diffracted wave to that of the incident wave):[10,12,14]

$$-i\frac{dX}{dZ}=X^2-2\eta X+1, \tag{1}$$

where

$$Z=\frac{\pi C}{\lambda}\left(\sqrt{\frac{\psi_H\psi_{\bar{H}}}{|\gamma_0\gamma_H|}}\right)z, \tag{2}$$

$$\eta=-\frac{(1+b)\psi_0+\alpha}{2C\sqrt{|b|\psi_H\psi_{\bar{H}}}}, \tag{3}$$

$$\psi_{0,H,\bar{H}}=-\frac{\lambda^2\gamma_e}{V\pi}F_{0,H,\bar{H}}, \tag{4}$$

$$\alpha=b(\theta-\theta_B)\sin 2\theta_B. \tag{5}$$

Here z is the distance in the crystal, being zero at the bottom of the layer and of positive values toward the surface, $b=-\gamma_H/\gamma_0$, where γ_0 and γ_H are the direction cosines of the incident and diffracted waves, respectively, θ and θ_B are the rocking angle and the Bragg angle, respectively, V is the volume of the unit cell, λ is the x-ray wavelength, F is the structure factor of the group of atoms in the unit cell, γ_e is the classical electron radius (2.818×10^{-5} Å), and C is the polarization factor which is equal to 1 and $\cos 2\theta$ for perpendicular and parallel polarized waves, respectively.

A. The kinematic approximation

In the kinematic approximation, the effects of multiple reflections are neglected. For a semiconductor layer thinner than a few thousand Å, this is a good approximation because this thickness is much less than the x-ray extinction length. In this approximation the quadratic term in Eq. (1) is omitted and the resultant equation can be solved analytically for a layer of constant η and arbitrary thickness and for a section in a layer where η can be considered to be constant. The solution is given by[6,10]

$$X_z=X_0e^{-i2\eta Z}+ie^{-i\eta Z}\left(\frac{\sin\eta Z}{\eta}\right), \tag{6}$$

where X_0 is the normalized amplitude ratio at the bottom of the layer and X_z is the ratio at the top. This equation can be used to simulate the diffraction profile of a multiple-layer crystal structure. Given θ_B, z, and ψ for each layer, one can then obtain the corresponding η and Z. The value of X at the crystal surface is then obtained by applying Eq. (6) recursively. The reflectivity, or the ratio of the intensity of the diffracted wave to that of the incident wave at the crystal surface, is given by

$$R=\left|\frac{b\psi_H}{\psi_{\bar{H}}}\right|\left|X\right|^2. \tag{7}$$

The rocking curve for a crystal is then given by R as a function of the glancing angle θ.

For (100) oriented III-V compounds, the first term in the numerator of Eq. (3) is negligible if θ deviates more than $\sim0.01°$ away from θ_B. For a single crystal layer with finite thickness z and with no incident x-ray beam from the bottom, the reflectivity at the surface of the crystal can be approximated by

$$R\simeq k\frac{\sin^2[(2\pi z\cos\theta_B/\lambda)(\theta-\theta_B)]}{(\theta-\theta_B)^2}, \tag{8}$$

where k is a constant. Equation (8) suggests that the diffraction profile of a single layer is similar to the optical far-field interference pattern of a single slit with slit size of $z\cos\theta_B$. The intensity maxima of the Pendellösung fringes occur when the condition $(2\pi z\cos\theta_B/\lambda)(\theta-\theta_B)=(m+1/2)\pi$ is satisfied for $m=0,\pm1,\pm2,\ldots$. The layer thickness can be obtained from this relation and is given by

$$z=\lambda/(2\Delta\theta\cos\theta_B), \tag{9}$$

where $\Delta\theta$ is the angular separation between adjacent maxima. For a single uniform epitaxial layer, this relation can give very accurate estimation of the layer thickness, as confirmed by other measurement techniques.

For a two-layered AB structure in which two layers of compositions A and B are put together, the reflectivity at the surface is approximated by

$$R \simeq k_1 \frac{\sin^2[(2\pi z_A \cos\theta_B^A/\lambda)(\theta-\theta_B^A)]}{(\theta-\theta_B^A)^2} + k_2 \frac{\sin^2[(2\pi z_B \cos\theta_B^B/\lambda)(\theta-\theta_B^B)]}{(\theta-\theta_B^B)^2} + \text{interference terms}, \quad (10)$$

where k_1 and k_2 are constant. The first and second terms are the reflectivities of layers A and B, respectively. When both A and B are very thick, the first two terms give two maxima. One occurs at the Bragg angle of layer A, θ_B^A, and the other at the Bragg angle of layer B, θ_B^B. Thus, the lattice spacing of B can be accurately determined if that of A is known. However, when layer A is very thick and layer B is very thin, the maximum due to the second term is comparable to the magnitudes of the tails of the rest terms at θ_B^B. The overall maximum due to B and the tails will thus shift toward the first maximum at θ_B^A. Determination of the lattice spacing directly from this peak will thus lead to an error. This is the origin of the Fewster and Curling effect.[15]

When the two-layered AB structure is grown on a thick substrate of composition A, with B embedded in A, it becomes an ABA structure. The reflectivity at the surface is approximated by

$$R=\left|\frac{1}{2}\left(\frac{1}{\eta_A}-\frac{1}{\eta_B}\right)e^{-i2\eta_A Z_A}(e^{-i2\eta_B Z_B}-1)+\frac{1}{2\eta_A}\right|^2. \quad (11)$$

We can see that when $\eta_B Z_B$ increases by a multiple of 2π, the reflectivity remains the same. This means that similar interference structures near θ_B^A can be obtained by changing the thickness of B by a multiple of $(d_B^{-1}-d_A^{-1})^{-1}$ or changing d_B by a multiple of d_B^2/z_B. These changes correspond to the motion of successive Pendellösung fringes across the Bragg peak of A. This is the origin of the uncertainties mentioned in Ref. 5.

It is worth noting that the reflectivities from side A and side B of the AB structure are identical when both A and B are very thin. This may give rise to another degree of uncertainty in the characterization of multilayered heterostructures.

B. Dynamical simulation

Although the kinematic approximation provides direct insight into the interference phenomena, it lacks in accuracy in detailed fitting of experimental rocking curves. The dynamical theory must be used especially when the thickness of the multilayered structure approaches the x-ray extinction length. One can solve the full dynamical equation given in Eq. (1) analytically and obtain the following recursion relation:[8,10,16]

$$X_z=\eta+\sqrt{\eta^2-1}\left(\frac{1+S}{1-S}\right), \quad (12)$$

where

$$S=\frac{(X_0-\eta-\sqrt{\eta^2-1})}{(X_0-\eta+\sqrt{\eta^2-1})}e^{i2Z\sqrt{\eta^2-1}}. \quad (13)$$

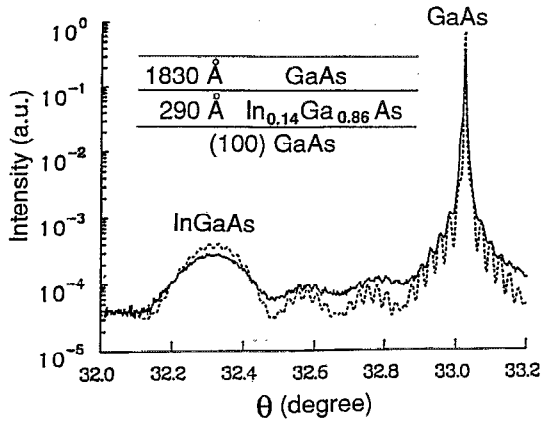

FIG. 1. Measured and calculated (004) rocking curves of a pseudomorphic GaAs/InGaAs heterostructure.

For a layer of infinite thickness, X_z reduces to

$$X_\infty=\eta-\text{sign}(\text{Re}[\eta])\sqrt{\eta^2-1}, \quad (14)$$

where Re[η] is the real part of η.

IV. DETERMINATION OF LAYER COMPOSITION, THICKNESS AND CRITICAL LAYER THICKNESS

Figure 1 shows measured (solid) and simulated (dashed) (004) x-ray rocking curves of a coherently strained InGaAs/GaAs heterostructure. The structure of the sample is shown in the inset. The rocking curve clearly shows the Bragg peaks from the GaAs and InGaAs layers and distinct Pendellösung oscillations from the cap layer modulated by slower oscillations from the InGaAs layer. With the aid of computer analysis, we can accurately extract the out-of-plane lattice constant of the InGaAs layer and the thickness of both layers without subjecting them to the ambiguity due to order multiplicity mentioned previously. With an additional asymmetric diffraction measurement, e.g., the (115) diffraction, the in-plane lattice constant of the InGaAs layer can also be determined.

Shown in Figs. 2(a) and 2(b) are the measured parallel and perpendicular lattice constants of the InGaAs layers of various compositions and thicknesses. The parallel lattice constants are measured along the $(1\bar{1}0)$ direction by $(1\bar{1}5)$ and $(\bar{1}15)$ asymmetric reflections. As can be seen, when the layer reaches a certain thickness, the parallel lattice constant increases and the perpendicular lattice constant decreases. These changes are due to the gradual strain relief process. If we define the thickness at which we see the onset of relaxation of the parallel lattice constant as the critical thickness, we obtain a plot of critical thickness versus indium composition as shown in Fig. 3. Also shown in Fig. 3 are the estimated critical thicknesses by the Matthews and Blakeslee force balance model[17] which is given by

$$h_c=\left(\frac{b}{m\pi f}\right)\left(\frac{1-\nu/4}{1+\nu}\right)\left[\ln\left(\frac{h_c}{b}\right)+1\right], \quad (15)$$

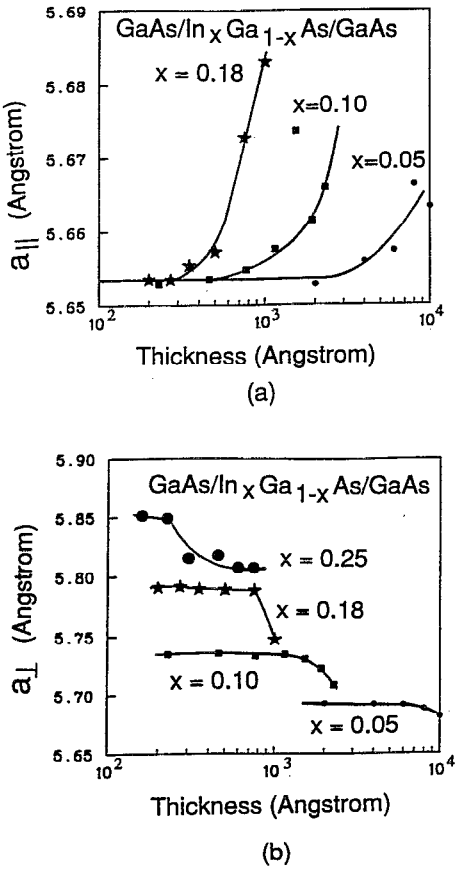

FIG. 2. Measured (a) parallel and (b) perpendicular lattice constants of InGaAs layers embedded in GaAs.

where Poisson's ratio ν, lattice constant a, and misfit strain f are functions of the indium composition, $m=4$ for a single epitaxial layer or an embedded layer with only the epilayer-substrate interface containing misfit dislocations (single-kink model) and $m=2$ for an embedded layer with dislocations introduced at both the epilayer-cap and epilayer-substrate interfaces (double-kink model). It is not clear which model should be used for an embedded

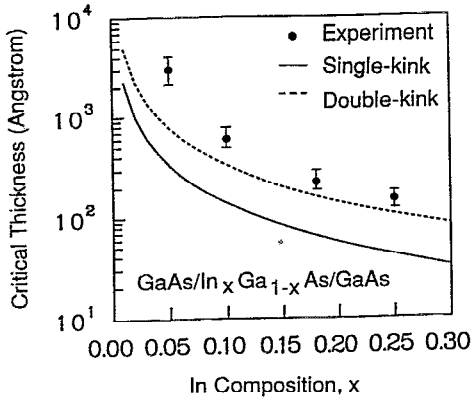

FIG. 3. Measured critical thicknesses of buried InGaAs layers as a function of indium composition.

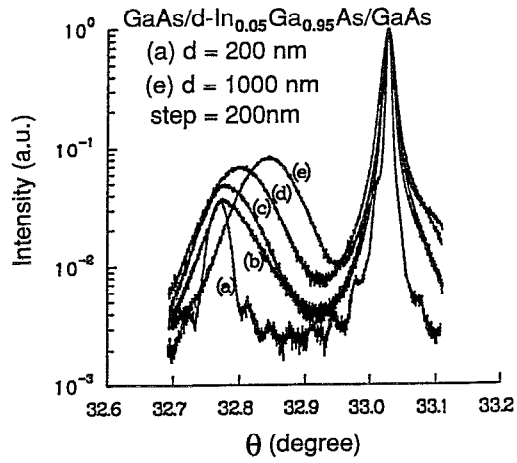

FIG. 4. Measured (004) rocking curves for buried $In_xGa_{1-x}As$ layers with various thicknesses. The broadened peaks and absence of Pendellösung fringes in curves (b) to (e) indicate the existence of strain relaxation.

strained layer. In fact, Chang[18] has studied misfit dislocations in $In_{0.07}Ga_{0.93}As/GaAs$ multiquantum well (MQW) structures by cross-sectional transmission electron microscope (TEM) micrographs. The results showed that dislocations occurred only at the epilayer-substrate interface. No matter where the misfit dislocations occur, both the single- and double-kink models failed to explain the measured critical thickness. The underestimation of the critical thickness in the force balance model might be due to the neglect of friction forces, surface stress, and stacking fault energy. Our measurements might also slightly overestimate the critical thickness since the initial dislocation generation may not lead to measurable strain relaxation.[19]

Misfit dislocations due to strain relaxation have dramatic effects on the x-ray diffraction pattern. As shown in Fig. 4, when the strain is coherent, the Bragg peaks are sharp and the interference pattern clearly shows the Pendellösung oscillations [curve (a)]. When strain starts to relax, the Bragg peaks are significantly broadened [curves (b)–(e)]. The Pendellösung fringes also disappear. The broadening of Bragg peaks might be attributed to the following reasons. First, the generation of misfit dislocations results in nonuniform distribution of the residual strain.[19] Therefore, the lattice constants are different in different regions. The total envelope of the strained-layer peak is thus broadened. The broadening of x-ray peaks may also be related to the presence of anisotropic tilting of lattice planes along dislocations.[20] The nonuniform distribution of lattice constants and the tilting of lattice planes can destroy the phase coherency of the diffracted waves, resulting in the disappearance of the interference pattern. The disappearance of Pendellösung fringes thus can be used as a sensitive probe of strain relaxation. In Fig. 3, the critical thicknesses for $x \lesssim 0.2$ are determined from lattice constants and Pendellösung patterns, while that for $x=0.25$ is determined from Pendellösung patterns solely. Interface roughness can also damp the oscillations. However, the concurrence of the disappearance of oscillations and strain

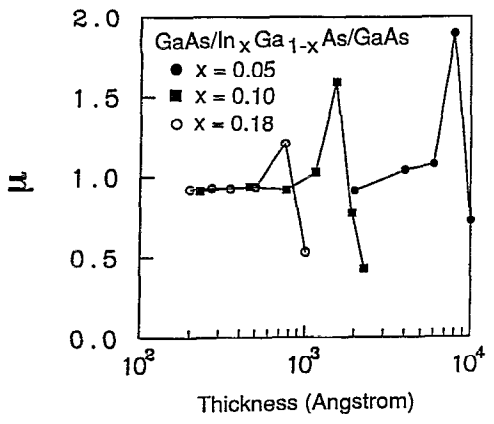

FIG. 5. Measured values of μ as a function of epitaxial layer thickness. Here $\mu=(a_\perp^e-a_o^e)/(a_o^e-a_\parallel^e)$.

relaxation in our measurements indicates that strain relaxation is the dominating factor.

V. STRAIN TENSOR

It can be shown that for a coherently strained epitaxial layer grown on (100)-oriented substrate, the off-diagonal components of the strain are zero and the diagonal components are given by:

$$\epsilon_{xx}=\epsilon_{yy}=\epsilon_\parallel=-\frac{a_o^e-a^s}{a^s},$$
$$\epsilon_{zz}=\epsilon_\perp=-\epsilon_\parallel/\sigma,\quad \sigma=\frac{c_{11}}{2c_{12}}, \tag{16}$$

where the superscripts e and s represent the epitaxial layer and the substrate, respectively, and the subscript o represent the native lattice constant. For the coherent strain case, $\epsilon_{xx}=f$, while for the partial strain relief case, a^s in Eq. (16) should be replaced by $a_\parallel^e$. If we define $\mu=(a_\perp^e-a_o^e)/(a_o^e-a_\parallel^e)$, then we expect μ to be equal to $1/\sigma$ when the strain is coherent. The value of μ as a function of epitaxial layer thickness for various In compositions is shown in Fig. 5. As expected, when the layer is pseudomorphic, $\mu\sim0.91$ which is equal to the theoretical value of $1/\sigma$. However, when the strain starts to relax due to increased thickness, μ deviates from $1/\sigma$ significantly, indicating that the elastic theory alone is insufficient to interpret the measured data.

These results have very important implications for the measurements of epitaxial layer composition by x-ray diffraction. In usual practice, one obtains the native lattice constant a_o^e of the epitaxial layer from measured $a_\perp^e$ and $a_\parallel^e$ according the elastic theory. Then the epitaxial layer composition is obtained from a_o^e by assuming that Vegard's law is valid (for III-V compounds). However, Fig. 5 suggests that a_o^e can be accurately measured only under these extreme conditions: (1) when the strain is completely coherent in which case the elastic theory can be applied; (2) when the strain is completely relaxed and $a_o^e=a_\perp^e=a_\parallel^e$ is valid.

VI. CONCLUSION

We have used the double-crystal x-ray rocking curve technique to determine the structural parameters of thin $In_xGa_{1-x}As$ layers embedded in GaAs. In this work we have measured and analyzed the x-ray data over a wide scan angle to cover the Bragg peaks of both GaAs and $In_xGa_{1-x}As$. This allows for the simultaneous determination of buried layer thickness and lattice constants without subjecting them to the ambiguity due to order multiplicity. The measurement results were analyzed by the dynamical diffraction theory. The critical thickness for an InGaAs layer embedded in GaAs obtained from x-ray data is measured to be larger than that predicted by the force balance model. Analysis of the strain tensor suggests that the elastic theory can be applied to an epitaxial layer only when the strain is completely coherent.

ACKNOWLEDGMENTS

This work is supported by the Office of Naval Research under Grant N00019-89-J1519 and a grant from Ford Motor Company. The authors acknowledge useful discussions with Professor J. Singh and Dr. H. Holloway.

APPENDIX

In the literature, both the Darwin–Prins[11] and the Taupin–Takagi[12,13] equations have been used to simulate the measured x-ray rocking curves. Analytic solutions have been obtained by Perkins *et al.*[21] for the former and by Halliwell *et al.*[8] and Hill *et al.*[16] for the latter. In this Appendix, we show that the difference equations of Darwin and Prins can be converted into the differential equations of Taupin and Takagi under the assumption that the crystal is a continuous medium.

We first consider the Darwin's difference equations as given by James.[11] We assume that the crystal consists of a series of parallel lattice planes with the adjacent planes separated at a distance a apart. We denote each plane by a serial number r, starting with the surface plane. T_0 and S_0 represent the amplitude of the incident and the reflected x-ray beams at the surface, respectively, and T_r and S_r represent the amplitude of the incident and the reflected beams, respectively, at a point just above the rth plane. The glancing angle between the incident beam and the atomic planes is θ. The waves reflected by the atoms in each plane are assumed to be in phase so that S_r is a plane wave whose angle is also θ relative to the atomic planes.

Let $-iq_H$ and $-iq_{\bar H}$ represent the reflection coefficients from the upper side and lower side of a single plane of atoms, respectively. They may be, but not necessarily, the same. Let $(1-iq_0)$ represent the transmission coefficient through a plane of atoms. $q_{0,H,\bar H}$ can be expressed as

$$q_0=-\frac{N a\lambda\gamma_e}{\sin\theta}F_0=-\frac{a\lambda\gamma_e}{V\sin\theta}F_0 \tag{A1}$$

$$q_{H,\bar H}=-C\frac{a\lambda\gamma_e}{V\sin\theta}F_{H,\bar H}, \tag{A2}$$

where N is the number of unit groups of atoms in unit volume V. Other symbols have the same meaning as mentioned in the text.

The waves at the rth and the $(r+1)$th planes are related by

$$S_r=-iqT_r+(1-iq_o)e^{-i\xi}S_{r+1}, \tag{A3}$$

$$T_{r+1}=(1-iq_o)e^{-i\xi}T_r-i\bar{q}e^{-i2\xi}S_{r+1}, \tag{A4}$$

where

$$\xi=\frac{2\pi a}{\lambda}(\sin\theta-\sin\theta_B). \tag{A5}$$

Equations (A3) and (A4) are the Darwin–Prins difference equations. Equation (A3) says that S_r is composed of the part of T_r reflected from the rth plane and the part of S_{r+1} transmitted through the rth plane. Equation (A4) is interpreted similarly. The second term on the right-hand side of Eq. (A4) corresponds to multiple reflections.

Substituting (A1) and (A2) into (A3) and (A4) and rearranging the equations, we get

$$\frac{S_{r+1}-S_r}{a}=i\frac{\lambda\gamma_e}{V\sin\theta}(CF_HT_{r+1}+F_0e^{-i\xi}S_r)-\frac{1}{a}(1-e^{-i\xi})S_r, \tag{A6}$$

$$\frac{T_{r+1}-T_r}{a}=-i\frac{\lambda\gamma_e}{V\sin\theta}(F_0e^{-i\xi}T_{r+1}+CF_{\bar{H}}e^{-i2\xi}S_r)+\frac{1}{a}(1-e^{-i\xi})T_{r+1}. \tag{A7}$$

Now we will assume that the crystal is a continuous medium and, therefore, the following statements are valid:

(1) The planar spacing a is very small ($a\to 0$).

(2) The difference between S_r and S_{r+1} for all r is so small that we can represent the series $(S_0,S_1,\ldots,S_r,S_{r+1},\ldots)$ by a continuous function $S(z)$, where z is the distance from the surface into the crystal. Similarly, we can represent the series $(T_0,T_1,\ldots,T_r,T_{r+1},\ldots)$ by a continuous function $T(z)$.

(3) The functions $S(z)$ and $T(z)$ are differentiable at all z in the crystal. Replacing ra by z, we can rewrite Eqs. (A6) and (A7) as

$$-\frac{i\lambda}{\pi}\gamma_H\frac{dS(z)}{dz}=C\psi_HT(z)+\psi_0S(z)-\alpha_HS(z), \tag{A8}$$

$$-\frac{i\lambda}{\pi}\gamma_0\frac{dT(z)}{dz}=\psi_0T(z)+C\psi_{\bar{H}}S(z)-\alpha_0T(z), \tag{A9}$$

where $\alpha_0=-2\gamma_0(\sin\theta-\sin\theta_B)$ and $\alpha_H=2\gamma_H(\sin\theta-\sin\theta_B)$. γ_0, γ_H, and $\psi_{0,H,\bar{H}}$ have their meaning as defined in the text. Equation (A8) and (A9) are the Taupin–Takagi differential equations. Let $Y=S/T$, then we can combine (A8) and (A9) and obtain

$$\frac{dY}{dz}=-i\frac{\pi}{\lambda\gamma_H}\{C\psi_{\bar{H}}Y^2+[(1+b)\psi_0+\alpha]Y+Cb\psi_H\}. \tag{A10}$$

For the symmetrical reflection, we can put $\gamma_0=-\gamma_H=\sin\theta_B$ and $\alpha=2(\theta-\theta_B)\sin 2\theta_B$. For asymmetric diffraction, γ_0 and γ_H must be replaced by the direction cosines of the incident and reflected beams with respect to the surface normal, respectively.

For convenience, we redefine z such that it is zero at the bottom of the layer and has positive value toward the surface. We also further define the following new complex variables:

$$X=\sqrt{\frac{\psi_{\bar{H}}}{|b|\psi_H}}Y, \tag{A11}$$

$$Z=\frac{\pi C}{\lambda}\left(\sqrt{\frac{\psi_H\psi_{\bar{H}}}{|\gamma_0\gamma_H|}}\right)z, \tag{A12}$$

$$\eta=-\frac{(1+b)\psi_0+\alpha}{2C\sqrt{|b|\psi_H\psi_{\bar{H}}}} \tag{A13}$$

then Eq. (A10) becomes

$$-i\frac{dX}{dZ}=X^2-2\eta X+1. \tag{A14}$$

[1] B. K. Tanner and M. J. Hill, Adv. X-ray Analysis **29**, 337 (1986).
[2] T. W. Ryan, P. D. Hatton, S. Bates, M. Watt, C. Sotomayor-Torrs, P. A. Claxton, and J. S. Roberts, Semicond. Sci. Technol. **2**, 241 (1987).
[3] C. R. Wie, J. Appl. Phys. **65**, 1036 (1989).
[4] X. Chu and B. K. Tanner, Appl. Phys. Lett. **49**, 1773 (1986).
[5] H. Holloway, J. Appl. Phys. **67**, 6229 (1990).
[6] V. S. Sperious and T. Vreeland, Jr., J. Appl. Phys. **56**, 1591 (1984).
[7] L. Tapfer and K. Ploog, Phys. Rev. B **33**, 5565 (1986); *ibid.* **40**, 9802 (1989).
[8] M. A. G. Halliwell, M. H. Lyons, and M. J. Hill, J. Cryst. Growth. **68**, 523 (1984).
[9] D. M. Vardanyan, H. M. Manoukyan, and H. M. Petrosyan, Acta Crystallogr. A **41**, 212 (1985).
[10] W. J. Bartels, J. Hornstra, and D. J. W. Loobek, Acta Crystallogr. A **42**, 539 (1986).
[11] R. W. James, *The Optical Principles of the Diffraction of X-rays* (Cornell University, Ithaca, 1965), Chap. 2.
[12] D. Taupin, Bull. Soc. Fr. Mineral. Crystallogr. **87**, 469 (1964).
[13] S. Takagi, J. Phys. Soc. Jpn. **26**, 1239 (1969).
[14] P. J. Burgeat and D. Taupin, Acta Crystallogr. A **24**, 99 (1968).
[15] P. F. Fewster and C. J. Curling, J. Appl. Phys. **62**, 4154 (1987).
[16] M. J. Hill, B. K. Tanner, M. A. G. Halliwell, and M. H. Lyons, J. Appl. Cryst. **18**, 446 (1985).
[17] J. M. Matthews and A. E. Blakeslee, J. Cryst. Growth **27**, 118 (1974).
[18] K. H. Chang, Ph.D. dissertation, the University of Michigan, 1989, Chap. 5.
[19] P. Y. Timbrell, J.-M. Baribeau, D. J. Lockwood, and J. P. McCaffrey, J. Appl. Phys. **67**, 6292 (1990).
[20] M. Grundmann, U. Lienert, and D. Bimberg, Appl. Phys. Lett. **55**, 1765 (1989).
[21] R. T. Perkins and L. V. Knight, Acta Crystallogr. A **40**, 617 (1984).